High resolution observations of free tropospheric humidity from METEOSAT over the Indian Ocean.

Rémy Roca, Hélène Brogniez, Laurence Picon and Michel Desbois
Laboratoire de Météorologie Dynamique, CNRS, Palaiseau,France

MEGHA-TROPIQUES 2nd Scientific Workshop, 2-6 July 2001, Paris, France.

Abstract

Water vapor is a central element of the tropical climate through its interactions with longwave radiation as well as through its forcing onto convective activity. The scales of interest for water vapor span the Hadley circulation and its subsiding dry branches down to mesoscale features of around 50km. The satellite observations from METEOSAT-5 over the Indian Ocean in the 6.3 microns band are used to derive an estimate of the free tropospheric relative humidity at 5x5 km resolution in order to better document the various scale of the moisture field.

The retrieval algorithm is similar to the operational algorithm run at EUMETSAT with slight modifications in the interpretation of the inverted signal. It relies on the use of local look up table and radiative transfer computations. The ancillary data needed for the algorithm are composed of the temperature profile taken from the ECMWF analysis. The final product is the weighting function weighted mean relative humidity over the free troposphere (FTH).

The algorithm is fully presented and is validated thanks to an ensemble of radiosondes acquired during the INDOEX campaign. It is shown that the satellite derived FTH is in excellent agreement with the in-situ measurements with a bias of -2.7% and a standard deviation of 6%. The calibration of the captor is further investigated and shown to agree with radiosondes simulated brightness temperatures within 0.5K ruling out the idea of a calibration induced bias. The full resolution FTH imagery reveals the dryness of the intertropical troposphere with value often below 10% as well as the strong horizontal gradients associated with the FTH fields. Perspectives in the frame of the MEGHA-TROPIQUES mission are given.

1 Introduction

Water vapor plays a key role in the climate of the Tropics through two major mechanisms:

• First, in the convective regions, its vertical distribution contributes to the inhibition of vertical motions. A very dry sounding in the troposphere will usually exhibits a strong inversion which prevents the air particle to consume the available energy. These dry tongues in the convectively active regions were shown to strongly interact with convection during TOGA-COARE (Brown and Zhang, 1997). The origin of these quite frequent dry air masses appears to

be extra-tropical associated with some instability of the subtropical jet streams. The distribution mid-tropospheric water vapor hence modulates convection. Examples of these dry intrusions are seen over the Warm Pool but also the Atlantic ocean and tropical Africa (Redelsperger, 2001 this issue) and were observed during INDOEX over the Indian Ocean as well.

• Second, water vapor acts as an important greenhouse gas in the atmosphere and is usually associated with a strong positive feedback mechanism on the surface temperature. Due to some non-linearities in the sensitivity of the outgoing longwave radiation to the vertical profile of water vapor, the low humidity regions have been shown to have the more potential leverage power on the climate (e.g., Spencer and Braswell, 1997). In the intertropical belt, these low humidity regions are found essentially in the upper troposphere over the ITCZ and the whole free troposphere over the subtropical large-scale subsiding regions. The latter, being extremely dry, were suggested to govern the tropical climate equilibrium, acting as fins that would allow excess energy to be efficiently radiated to space (Pierrehumbert, 1995). The tight connection between large scale transport and the moisture distribution in these subsiding regions was recently demonstrated (Pierrehumbert and Roca, 1998) and the role of the fine scale structures highlighted. The role of the former region have been central to a large polemical debate in the community over the last decade (Lindzen's negative feedback theory). At the intraseasonal scale, the variability of the upper tropospheric humidity field over the Indian Ocean explains a large fraction of the clear sky greenhouse effect variability (Roca et al., 2001). Tropical deep convection can be thought of as the source of moisture for these two regions.

In order to further our understanding of the interplay between convection, dynamics and water vapor in the climate, the crucial link between these systems need to be fully captured. On the observations side, one basically needs to scale down to the distribution of moisture at mesoscale, both in the immediate environment of the organized convective clouds as well over the extended subtropical dry zones. By the time SAPHIR data are available, the MEGHA-TROPIQUES mission can gain insight from readily available infrared imager data analysis. The present paper offers one of such insight into the upper tropospheric humidity distribution using the full resolution (5x5km) observations of the METEOSAT-5 so-called "water vapor" channel.

2 Design and validation of the algorithm

2.1 Design

The present algorithm extends the Upper Tropospheric Humidity (UTH) operational algorithm of EUMETSAT (Schmetz et al., 1995) to the full resolution with slight modifications drawn on to the interpretation of the UTH parameters. It is based on the relationship between the mean relative humidity over a layer of the troposphere and the brightness temperature. Indeed Soden and Bretherton (1993) introduced the following relationship based on a simplified radiative transfer theory:

$$ln(p_0\overline{RH}/cos\theta) = aT_B + b \tag{1}$$

where p_0 is a normalizing parameter equal to the ratio of the pressure of the 240K isotherm to 300 hPa which allows to account for the latitudinal and seasonal variation of the tropical lapse

rate (Engelen and Stephens, 1998). The $\overline{RH}$ corresponds to the relative humidity (with respect to water) averaged over a given layer of the troposphere whose the satellite captor is sensitive to. In the EUMETSAT approach, this layer is 600-300 hPa and in the present work it is detailed in the next section. θ is the satellite viewing angle and T_B the 6.3 microns brightness temperature. The coefficients a and b are the linear fitting coefficient. While the simplified formulation of the relationship of the T_B to the humidity has been used by a number of authors, the main differences arises from the way to compute the fitting coefficients. Soden and Bretherton (1993) obtain the coefficients from a global fit using one month of observations of GOES-7. Similarly, Spencer and Braswell (1997) inverted the 183GHz signal of SSM/T2 using equation 1 and an ensemble of radiosondes. Unlike the global approach, Schmetz et al. (1995) build a look up table where the fitting coefficients are computed *locally* using ECMWF forecasts. We here follow the latter approach which better takes into account the high frequency variability of the lapse rate.

The local look up table relies onto radiative transfer computations that are performed using an improved version of the narrow band model of Morcrette and Fouquart (1985). The code describes the METEOSAT spectral region (5.7-7.1 microns) using 10 unevenly spaced intervals. The filter function of the instrument is explicitly introduced in the computation as well as the geometry of the observations. Despite not including the water vapor continuum effect over this strong absorption band which could impact the retrieval (Soden et al., 2000), the model was shown to agree with the code used at EUMETSAT for former operational calibration within 0.5K over a wide range of atmospheric situations (Roca, 2000b). The weighting function is computed at the time as the brightness temperature.

2.2 Result for a standard atmosphere

The figure 1 shows the expected linear relationship between the brightness temperature and the logarithm of the relative humidity in a layer of the atmosphere. Computations are performed at nadir with $p_0 = 1$ for 10 values of the mean profile.

The linearity is excellent with a slight departure for the driest cases (RH=1%). This indicates that for these simplified profiles of relative humidity, the inversion model is performing very well.

2.3 Interpretation of the Free Tropospheric Humidity (FTH)

In the case of more realistic profiles of relative humidity, some caution need to be taken in order to interpret properly the retrieved relative humidity. Figure 2 shows the weighting function of the METEOSAT-5 water vapor channel for the standard tropical atmosphere. The weighting function is wide and peaks around 350 hPa. The sensitivity is significant over the 600-200 hPa layer, while the humidity above 200 hPa do not contribute to the measured signal. Similarly the moisture below 800 hPa do not influence the METEOSAT-5 radiance.

In consequence, the signal measured by the satellite corresponds to the mean relative humidity over the layer where the sensitivity of the captor is non zero. Recall that the width, peak altitude are function of the thermodynamical profile under considerations as well as the geometry of view. We hence define the Free Tropospheric Humidity (FTH) as the weighting function weighted mean relative humidity over the whole free troposphere (800-100 hPa). Because of

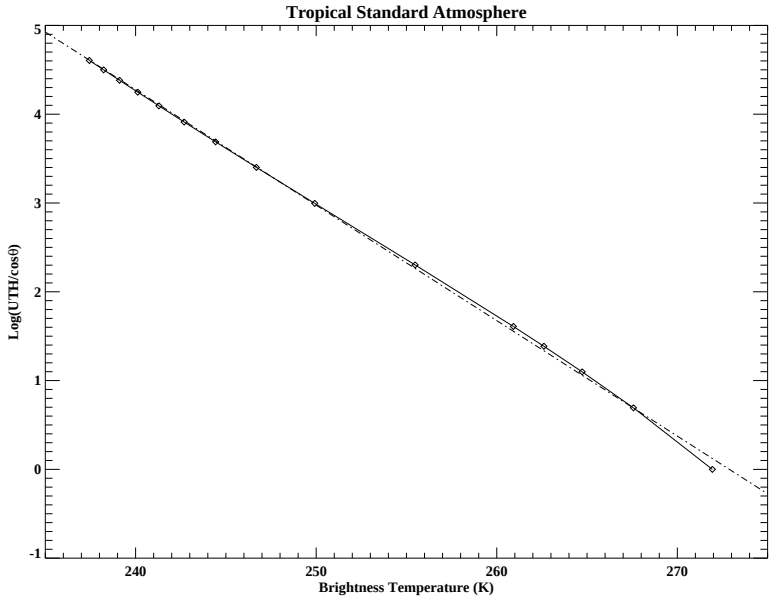

Figure 1: $\log(UTH/cos\theta)$ *as a function of the WV brightness temperature for a tropical standard atmosphere temperature profile. The relative humidity of the free troposphere (800-100hPa) is fixed at the values of 1,2,3,4,5,10,20,...,100% from right to left. Computations performed at nadir geometry. The value indicates the FTH corresponding to the standard tropical relative humidity profile. Dash line is the linear regression fit.*

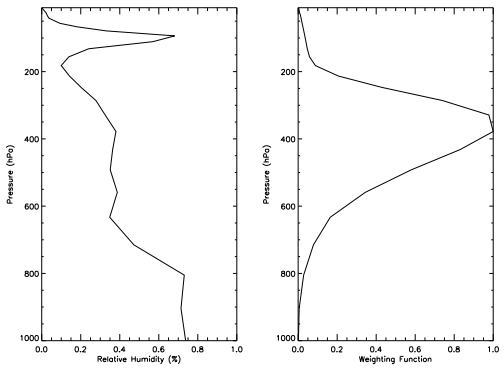

Figure 2: *Left: The tropical standard profile of relative humidity. Right: METEOSAT-5 WV channel weighting function for a standard tropical atmosphere seen at nadir.*

the strong linearity, only 2 radiative computations per temperature profile are needed to obtain the fitting coefficients. These are performed using a dry (5%) and moist (50%) constant profile of relative humidity over the 800-100 hPa layer which allows to span the range of usually encountered moisture conditions. The sensitivity of the retrieval to the choice of the dry and moist values is very weak.

2.4 Validation of the algorithm

Prior to the evaluation of the satellite product which encompasses different sources of uncertainties (ancillary data, calibration, algorithm bias), we briefly present the intrinsic behavior of the algorithm which is estimated using the ensemble of radiosondes.

2.4.1 INDOEX Radiosondes

During the INDOEX campaign, radiosondes were launched every 6 hours from the island of Hululé, Rep. of Maldives (4.96N,73.5E) as well as from the Ron Brown vessel which travelled over the Ocean during the campaign. The full resolution soundings were acquired at NCAR and were subsampled over 31 pressure levels to ease their manipulation and radiative transfer computations. Furthermore, an in-house quality checking was applied on the data in order to remove soundings that exhibited supersaturation in the free troposphere as well as extremely low values (RH$<$0.5%). Given that the retrieval is restricted to the clear sky areas, the METEOSAT cloud classification of Roca et al. (2001) is further used to filter out the scenes potentially contaminated with upper level cloudiness. The matching is performed at $\pm$ 15 minutes, 50km. The final database is composed of 215 soundings representative of the situations encountered over the Indian Ocean during the winter monsoon.

2.4.2 Results

The intrinsic behavior of the algorithm is assessed by comparing the radio soundings weighting function weighted relative humidity with that obtained from the inversion based on the brightness temperature simulated from the sounding. Figure 3 shows the scatter plot and the histogram of the difference between these two estimates of FTH.

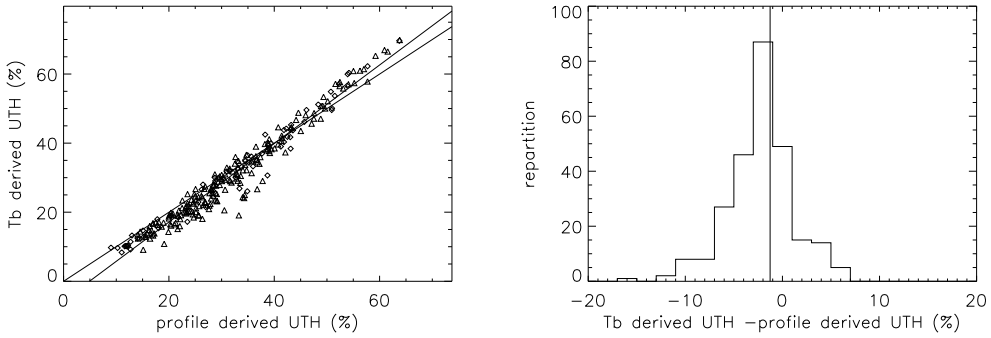

Figure 3: *Comparison between the radiosondes derived FTH and the brightness temperature derived FTH for the ensemble of radiosondes of INDOEX. Left: Scatter plot (correlation:0.97). Right: histogram of the difference. Bias -1.3%, standard deviation 3.3%. Diamonds correspond to the Hululé soundings while triangles correspond to the RonBrown vessel soundings.*

The comparison indicates that the algorithm provides an excellent estimate of FTH. The correlation is high, the scatter is low (standard deviation of 3.3%) and the fit shows a very small double bias. A slight underestimation prevails for the dry part of the ensemble of situations while a slight overestimation is found over the moistest cases. The critical value for the sign

of the bias is 50%. Below this value, the algorithm slightly, but systematically, underestimates FTH. The overall bias is very low (1.3%). Similar estimates of the algorithm behavior are found when using ECMWF water vapor profile as database instead of the soundings.

3 The METEOSAT-derived FTH product

The satellite product relies on the use of the ECMWF temperature profile for the building of the look up tables. This ancillary data set can impact the retrieval quality as well as the calibration of the instrument.

3.1 The local look up table from ECMWF analysis

The local look up table are constructed using the ECMWF analysis at a spatial resolution of 0.5x0.5 degrees every 6 hours. Up to March 9th, 31 levels are used in the radiative computations and after the 50 levels available are used. For each pixel of METEOSAT, the closest neighbor in the analysis in space and time is found to provide the fitting coefficients for the inversion. The uncertainty stemming from the use of these temperature profile is discussed in the following sections.

3.2 The WV channel calibration

The absolute calibration of the METEOSAT water vapor channel can also impact the retrieval. Briefly, the numerical raw counts measured by the captor are linearly related to a set of radiances computed from radiosondes. The final set of calibration coefficient depends upon the radiative transfer model and the radiosondes. From the beginning of the operation of METEOSAT up to nowadays, much variation of the quality of this vicarious method were noticed (see Roca, 2000a for a review) and were recently corrected for the nominal satellite ISCCP archive from 1983 to 1995 (Picon et al., 1999). Concerning the METEOSAT-5 spacecraft, detailed comparisons and inter satellites calibration exercises indicates that, especially over the INDOEX period, the calibration of the sensor was particularly stable and close to consensual estimates (Tjemkes et al., 2001). Figure 4 shows the scatter diagram of the observed brightness temperature versus the brightness temperature simulated from our radiation code and radiosondes dataset.

The correlation is high (R=0.88) and the linearity is good. The total bias is 0.5K, the observations being warmer than the simulation. The scatter is low with a standard deviation of 1.8K. Note that is the warmest case (WVEBBT $>$ 253K), corresponding to the dry end of the FTH spectrum, the satellite temperature are overall warmer than the simulations by around 1K which implies a small underestimation of the product there. More generally, by differentiating equation 1, the relative error in FTH due to a absolute error in T_B reads

$$\frac{p_0}{cos\theta}\frac{\Delta FTH}{FTH} = a\Delta T_B \tag{2}$$

Typical values for a range from -0.106 to -0.225 and average around -0.123. So that in the case of the standard atmosphere seen at nadir, the calibration bias induces a relative error on FTH around 5%. Most of the satellite derived FTH errors should hence be associated with the

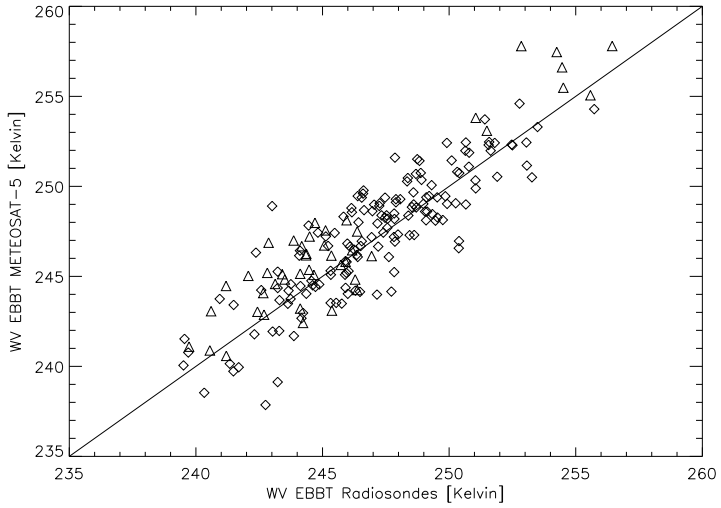

Figure 4: *Scatter diagram of observed vs simulated WV channel brightness temperature. Diamonds correspond to the Hululé soundings while triangles correspond to the RonBrown vessel soundings. Only clear sky scenes. 215 points form the diagram. R=0.88. Bias = 0.46K. Standard deviation: 1.8K*

convolution of the intrinsic bias of the algorithm and the use of ECMWF temperature profiles for the building of the look up table, ruling out strong calibration effect onto the product.

3.3 Evaluation of the product

The sum of the intrinsic errors of the algorithm plus the use of ancillary data is estimated by comparing the weighting function weighted relative humidity from the radiosondes database with the satellite derived FTH. Figure 5 shows the scatter diagram of these two parameters.

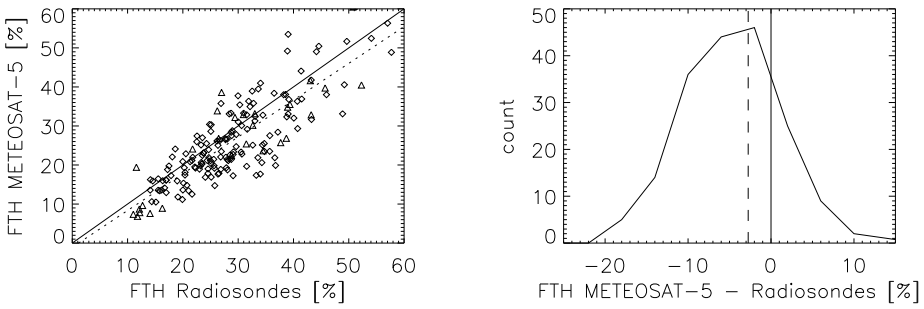

Figure 5: *Scatter diagram of satellite derived FTH versus the radiosondes estimated FTH. Diamonds correspond to the Hululé soundings while triangles correspond to the RonBrown vessel soundings. Only clear sky scenes. Number of points: 215. R=0.84. Bias=-2.7%. Standard deviation 5.8%*

In the low humidity regime, the product suffers from a slight underestimation of the driest cases by 3-4% which might be associated with the slight overestimation of the calibration over

the warmest brightness temperature. In the other part of the spectrum, the satellite derived FTH agrees well with the radiosondes with a slight average underestimation (2.7%). The standard deviation of the product versus the in-situ estimates is also low around 6%. The distribution of the difference (Figure 5 b) confirms the slight underestimation and the low bias. The final product quality closely resembles the intrinsic algorithm behavior but for a more negative bias which could be attributed to the ancillary data. Indeed most of the retrieved observations of FTH are lower than the 50% threshold previously mentioned for which the behavior of the retrieval tends to systematic slight underestimation. Overall, the satellite derived FTH appears in very good agreement with the independent in-situ estimates.

4 Example of High Resolution FTH imagery

Figure 6 shows the resulting FTH image deduced from the raw METEOSAT measurements and the algorithm for the 15th of February, 1999 at 12:00Z over the whole INDOEX region. The cloudiness which could interfere with the 6.3μm measurements, that is, mid to upper level clouds have been flagged in white. The cloud classification procedure from which this information is extracted is detailed in (Roca et al., 2001).

The image reveals the extreme dryness of the free troposphere over the Indian Ocean. Even though the product was previously shown to underestimate the FTH in the driest cases, the methodological and calibration bias is only of a few percents and cannot explain the large areas found with value less than 10%. Comparison with similar layered relative humidity products obtained from the microwave measurements of the SSM/T2 instrument should provide a way for increasing our confidence in these absolute values. The moistest areas (FTH $\sim$ 50%) are found to cover only a small fraction of the tropical region under consideration and is confined to the immediate environment of the mesoscale convective systems. The maximum value of FTH nevertheless do not exceed 55-60%. Recall that the relative humidities are here computed with respect to liquid water. Such values are close to saturation with respect to ice water in the upper troposphere. The second main feature that is exhibited by the FTH field is the extreme magnitude of the spatial gradients. Saturation and very low humidity are separated in many cases by only around 50km.

The high resolution retrieved distribution of mid-to-upper tropospheric relative humidity shown here is very consistent with the fact that, over the intertropical belt air masses are subsiding everywhere but in the convective towers which cover a small fraction of the whole area. Convection acts to moisten locally the upper troposphere as advocated in Roca et al. (2001) amongst others. The quantitative estimation of the local impact of convection could benefit from the technique proposed by (Udelhofen and Hartmann, 1995) where UTH is related to the distance to cloud edges, even though the role of transport in building the WV field should be taken into account. The filamentary structures reveals by the satellite product is one signature of the role of dynamics in shaping up the moisture distribution. These observations could be used to validate the very high resolution computations of water vapor relying on the chaotic advection hypothesis proposed by Pierrehumbert (1998).

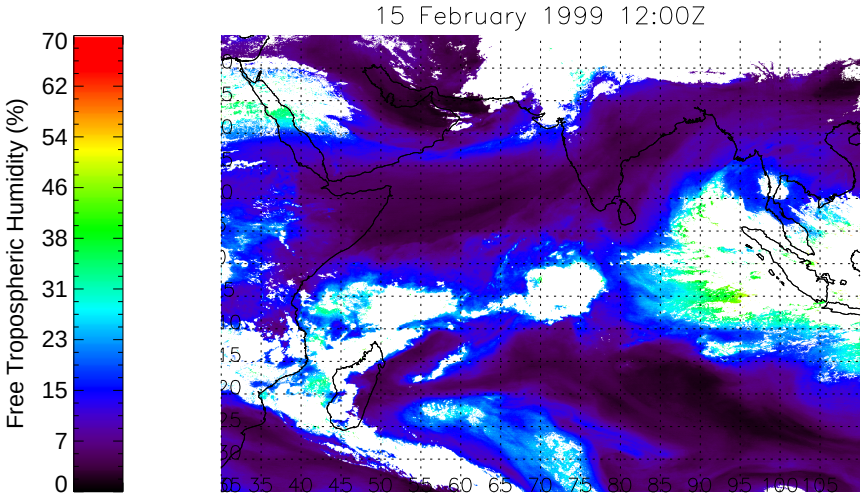

Figure 6: *Free Tropospheric Humidity for the 15th of February, 1999 at 12:00Z. Mid to upper level cloudiness is colored in white.*

5 Conclusions

The METEOSAT-5 observations in the 6.3 microns band are used to interpret the signal in terms of weighting function weighted relative humidity over the free troposphere (800-100 hPa). The algorithm is similar to the one operationally run at EUMETSAT. It relies simply through a linear fit the brightness temperature to the FTH. The intrinsic behavior of the algorithm is evaluated thanks to a ensemble of radiosondes. It shown to provide an excellent inversion. The satellite product derivation relies on the use of ancillary data (ECMWF temperature profiles) and is shown to compare very well with the radio-soundings with a bias of 2.7% and standard deviation of 6%. The high resolution FTH imagery reveals the strong horizontal gradients in the free tropospheric moisture field as well as the extreme dryness of the subtropical atmosphere with integrated values lower than 10%. The MEGHA-TROPIQUES mission through the SAPHIR instrument will provide the needed vertical description at high spatial resolution of the moisture field. The SAPHIR instrument will furthermore be of strong interested because of its soundings capabilities which in the microwave should allow to get sensitive information in the very near environment of clouds. By then, the availability of the present high resolution observations will be used to better understand the moisture-dynamics-convection relationships.

Acknowledgements Most of this work was performed in the frame of the second author (HB) master's thesis from the University of Paris 7 Denis Diderot. The never weakening efforts with data and CPU management of Jean-Louis Monge and the Climserv system are greatly

acknowledged.

6 References

Brown R.G. and Zhang C., 1997, Variability of mid-tropospheric moisture and its effect on cloud top height distribution during TOGA-COARE, J. Atmos. Sci., 54, pp 2760-2774.
Engelen R.J. and Stephens G.L, 1998, Comparison between TOVS/HIRS and SSM/T2 derived upper tropospheric humidity, Bull. Am. Met. Soc., 79, 12, pp 2748-2751.
Morcrette JJ. and Fouquart Y., 1985, On systematic errors in parametrized calculations of longwave radiation transfer, Q.J.R. Meteorol. Soc., 111, pp 691-708.
Picon L., Serrar S., Desbois M., Roca R. and Monge J.-L., 1999, Homogeneity of the METEOSAT water vapor data from 1983 to 1994 , EUMETSAT Contract, EUM/CO/98/606/HW.
Pierrehumbert R.T., 1998, Lateral mixing as a source of subtropical water vapor, Geophysical Research Letters, vol. 25, pp 151-154.
Pierrehumbert R.T. and R. Roca, 1998, Evidence for control of atlantic subtropical humidity by large scale advection. , Geophysical Research Letters, vol. 25, pp 4537-4540.
Redelsperger JL., 2001, Issues in tropical MCS understanding in the megha-tropiques context, 2nd MEGHA-TROPIQUES scientific workshop, July 2-6, Paris, France, this issue.
Roca R, 2000a, Contribution à l'étude de la convection, de la vapeur d'eau et de leurs interactions dans les Tropiques l'aide d'observations satellites et de modèle, PhD of the University of Paris 7.
Roca R, 2000b, Validation of GCMs cloudiness using METEOSAT observations, ECMWF/EuroTRMM Workshop on the Assimilation of precipitation and cloud radiances in NWP models, Reading, UK, 6-10 November, in press, 20 pp.
Roca R, M. Viollier, L. Picon and M. Desbois, 2001, A multi satellite analysis of deep convection and its moist environment over the Indian Ocean during the winter monsoon. , J. Geophys. Res, INDOEX special issue, in press.
Schmetz J., C. Geijo, W. Menzel, K. Strabala, L. van de Berg, K. Holmund, and Tjemkes S., 1995, Satellite observations of upper tropospheric relative humidity, clouds and wind field divergence, Contr. to Atmos. Phys., 68, pp 345-357.
Soden B.J. and F.P. Bretherton, 1993, Upper tropospheric humidity from the GOES 6.7 microns channel: method and climatology for July 1987, J. Geophys. Res., 98, pp 16669-16688.
Soden B.J. and 22 co-authors, 2000, An intercomparison od radiation codes for retrieving upper tropospheric humidity in the 6.3 microns band: a report from the first Gvap workshop, Bull. Am. Met. Soc., 81, 4, pp 797-808.
Spencer R and Braswell W, 1997, How dry is the tropical free troposphere ? Implications for global warming theory, Bull. Am. Met. Soc., 78, pp 1097-1106.
Tjemkes S.A., Konig M., Lutz H-J., van de Berg L., and Schmetz J., 2001, Calibration of METEOSAT water vapor channel observations with independent satellite observations, J. Geophys. Res., 106, pp 5199-5209.
Udelhofen P. and Hartmann D., 1995, Influence of tropical cloud systems on the relative humidity in the upper troposphere, J. Geophys. Res., 100, pp 7423-7440.